analytical chemistry

Article

pubs.acs.org/ac

Study of the Interactions of *Fusarium virguliforme* Toxin FvTox1 with Synthetic Peptides by Molecular Simulations and a Label-Free Biosensor

Bailin Zhang,[†] Bing Wang,[‡] Andres W. Morales,[†] Jonathan Scudder,[†] Madan K. Bhattacharyya,[‡] and Jing Yong Ye*[,†]

[†]Department of Biomedical Engineering, University of Texas at San Antonio, San Antonio, Texas 78249, United States

[‡]Department of Agronomy, Iowa State University, Ames, Iowa 50011, United States

ABSTRACT: *Fusarium virguliforme* is a soil borne pathogen that causes sudden death syndrome (SDS) in soybean plants. This pathogenic disease may result in severe soybean yield suppression and can cause serious economic harm. It has been shown that the FvTox1 toxin produced by the pathogen may be the root cause of foliar SDS. Anti-FvTox1 single-chain variable fragment antibody expressed in transgenic soybean plants was shown to neutralize the FvTox1 toxin involved in foliar SDS development. Here, we have investigated the binding affinities of FvTox1 with four FvTox1-interacting peptides of 7 to 12 amino acids identified from phage display libraries using both bioinformatics-based molecular simulations and label-free bioassays with a unique photonic crystal biosensor. Results from the molecular simulations have predicted the interaction energies and 3-dimensional (3D) structures of FvTox1 and FvTox1-interacting peptide complexes. Our label-free binding assays have further provided the interaction strength of FvTox1 with four different FvTox1-interacting peptides and experimentally confirmed the simulation results obtained from bioinformatics-based molecular calculations.

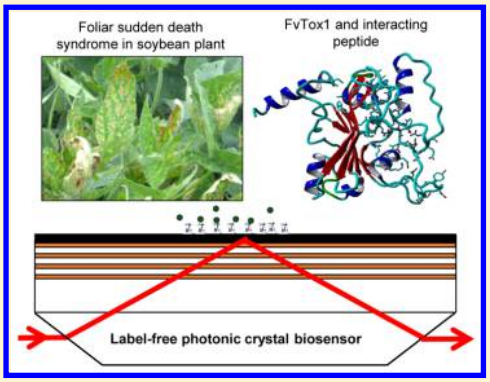

The United States leads the world in soybean production, yielding over $38 billion worth of soybean crops annually. However, pathogenic diseases, such as sudden death syndrome (SDS), can cause soybeans to suffer serious yield suppression.[1] Foliar SDS, a major threat to soybean production, is caused by *Fusarium virguliforme*, a soil-borne pathogen that produces FvTox1 toxin. Recent gene knockout experiments revealed that FvTox1 is a major virulence factor for foliar SDS.[2] Compared to the wild type isolate, Mont-1, it was discovered that *F. virguliforme* mutants lacking the *FvTox1* gene have reduced foliar SDS by approximately 3-fold.[2] Furthermore, expression of a single-chain variable fragment (scFv), Anti-FvTox1-1 antibody, in transgenic soybean plants was demonstrated to be effective for enhancing foliar SDS resistance.[3] However, because the antibody gene was created from a mammalian hybridoma cell line, it is not suitable for human consumption. Recently, four FvTox1-interacting peptides were identified from three M13 phage libraries.[4] In an M13 phage library, synthetic oligonucleotides were fused with a coat protein gene to have a library of recombinant fusion peptides displayed on the surface of the engineered bacteriophage. The FvTox1-interacting peptides may strongly bind to FvTox1 altering its function to cause foliar SDS. In this investigation, we studied the interactions of the isolated FvTox1-interacting peptides with FvTox1 using a bioinformatics-based molecular simulation method and an experimental binding assay with a label-free biosensor.

To understand the molecular basis of protein interactions and its functions, the 3-dimensional (3D) structure of a protein is of critical importance. Experimentally solving protein structures according to a protein sequence is a long and expensive process. Computational prediction of structures from a sequence of amino acids is now emerging as a promising alternative method. This method is showing huge potential to predict the structures of newly acquired sequences. This method is generated on the basis of crystal structures of proteins to predict structures of proteins with similar sequences.[5−7] On the basis of the predicted structures, the protein−protein and protein−peptide interaction energy can be calculated.

To verify the prediction of protein−protein interactions from computational methods, one can experimentally investigate protein−protein/peptide interactions using traditional assay technologies with fluorescence labeling or affinity tags. Although these methods are of high sensitivity, they are generally time-consuming and may possibly alter molecular functions due to the addition of fluorescent tags. Alternatively, label-free methods that allow direct measurements of molecular bindings without fluorescent tags may be utilized to study protein−protein interactions.[8,9] The most successfully commercialized label-free technologies are surface plasmon resonance (SPR)-based bioassays, although they still face challenging issues in achieving sufficiently high sensitivity for certain applications.[10]

Received: June 30, 2015
Accepted: February 9, 2016

DOI: 10.1021/acs.analchem.5b02442
Anal. Chem. XXXX, XXX, XXX−XXX

The photonic crystal structure-based technology utilized in this paper offers superior detection sensitivity as demonstrated in our previous studies.[11−15] A detection limit of 6×10^{-5} nm for an averaged molecular layer thickness, or 0.06 pg mm^{-2} analyte molecules, or a refractive index resolution of 3×10^{-8} refractive index unit (RIU) has been achieved with our biosensor based on a photonic crystal structure used in a total-internal-reflection (PC-TIR) configuration, which shows over 10-fold higher sensitivity compared with an SPR sensor.[15] The increased sensitivity stems from the sharp resonant condition of the open optical microcavity that is formed with the PC-TIR configuration.[11−15] In this paper, we report the binding affinities of FvTox1 with four peptides identified as FvTox1-interacting peptides from phage display libraries using both bioinformatics-based molecular simulations and label-free bioassays with the PC-TIR sensor.

SIMULATION AND EXPERIMENTAL METHODS

Bioinformatics-Based Molecular Calculation. Since experimentally solving structures of biological molecules to identify interacting peptides can be a long and expensive process, we have utilized an alternate bioinformatics approach to predict the structures of FvTox1 and FvTox1-interacting peptides, as well as their interaction energies. The sequences of FvTox1 and the four peptides are listed in Table 1. DNA molecules encoding each of the four peptides, viz., Pep 1, Pep 2, Pep 3, and Pep 4, were cloned in the expression pET 41(a+) vector and expressed in *E. coli* as fusion proteins.

We first used (PS)^2, an automatic protein structure prediction server,[6] to calculate the 3D molecular structures of FvTox1 and the four peptides directly from their amino acid sequences. The (PS)^2 server uses a computationally effective consensus strategy in two ways: a template selection combining PSI-BLAST (Position-Specific Iterative Basic Local Alignment Search Tool) and IMPALA (Integrating Matrix Profiles and Local Alignments) and a target-template alignment integrating PSI-BLAST, IMPALA, and T-Coffee (a multiple sequence alignment package). This server was tested for all comparative modeling targets in CASP6 (Critical Assessment of Techniques for Protein Structure Prediction),[16] and its predictions have been proven to be more accurate when compared to other automatic servers based on the GDT_TS (Global Distance Test Total Score) Score.[7] Structures with expectation values (E-value) of less than 10^{-2} and ultimately selecting predicted structures with the lowest E-value allowed the selected structures to be more accurate.

The structures of the protein FvTox1 and FvTox1-interacting peptides fusion proteins (Table 1) were used to calculate docking strengths in order to predict the putative structures of FvTox1−FvTox1-protein complexes. The FvTox1 with FvTox1-protein docking was performed on the ClusPro server, which offers one of the best methodologies for predicting protein−protein docking.[17−20] For each FvTox1−FvTox1-protein pair, the top 20 ranked predicted putative complex structures based on cluster sizes were selected for calculations of their interaction energies to further optimize the prediction of the structures. We utilized FoldX,[21−23] a molecular modeling algorithm, to compute the interaction energies of FvTox1 with different peptides. FoldX allows one to obtain the interaction energy of an FvTox1-Peptide (F−P) complex by calculating the Gibbs energies of both the complex (ΔG_{FP}) and the two separated molecules.

The formula for Gibbs free energy of a protein complex is

$$\Delta G = a\Delta G_{vdw} + b\Delta G_{solvH} + c\Delta G_{solvP} + \Delta G_{wb} + G_{hbond} + \Delta G_{el} + dT\Delta S_{mc} + eT\Delta S_{sc}$$

Table 1. Sequences of FvTox1 and Four FvTox1-Interacting Peptides[a]

name	sequence of the recombinant protein	M_w (kDa)	pI
FvTox1	MKSTFTLAALSLFASQCLAASVDMWSAPLSARSAARYEPIDPEVIKSRLGTTPEEYDPENRHAGMVYFCREENWGPPCFVYYPELEYTCSELGPE-LAGHVGSVFVEAGAICRMATLSAQDRCAPIEFFAWPETAAGWPDLLQRDGPDGKGKLGDETAHFTCECTNCVRNPQ	18.8	4.63
FvTox1-Protein 1	MRGSHHHHHHGMASMTGGQQMGRDLYDDDDKDRWGSGGGGSGGGGSGGGGS**SYLPETIYEYRL**GGGGS	6.9	5.99
FvTox1-Protein 2	MRGSHHHHHHGMASMTGGQQMGRDLYDDDDKDRWGSGGGGSGGGGSGGGGS**VENKTRYHDREV**GGGGS	6.9	6.34
FvTox1-Protein 3	MRGSHHHHHHGMASMTGGQQMGRDLYDDDDKDRWGSGGGGSGGGGSGGGGS**HEGAWHNYARSV**GGGGS	6.8	6.41
FvTox1-Protein 4	MRGSHHHHHHGMASMTGGQQMGRDLYDDDDKDRWGSGGGGSGGGGSGGGGS**SNGRVAD**GGGGS	6.1	6.25

[a]FvTox1-Protein 1, recombinant protein containing FvTox1-interacting Pep 1, SYLPETIYEYRL (shown in bold font); FvTox1-Protein 2, recombinant protein containing FvTox1-interacting Pep 2, VENKTRYHDREV (shown in bold font); FvTox1-Protein 3, recombinant protein containing FvTox1-interacting Pep 3, HEGAWHNYARSV (shown in bold font); FvTox1-Protein 4, recombinant protein containing FvTox1-interacting Pep 4, SNGRVAD (shown in bold font). The recombinant proteins were expressed in *E. coli* using the expression vector of pET 41(a+). Individual recombinant proteins were purified using a GST column followed by digestion with thrombin (Novagen, Madison, Wisconsin, USA).

DOI: 10.1021/acs.analchem.5b02442
Anal. Chem. XXXX, XXX, XXX−XXX

where the van der Waals contribution is represented by ΔG_{vdw}, while ΔG_{solvH} is the solvation energy change for hydrophobic groups. ΔG_{solvP} denotes polar groups during a protein's transition from an unfolded to folded state. G_{hbond} signifies hydrogen-bond energy. ΔG_{wb} stands for water bridge energy. ΔG_{el} corresponds with the electrostatic interaction contribution. ΔS_{mc} is the phi-psi contribution from a statistical analysis, while ΔS_{sc} represents the entropic cost of fixing a side-chain in a particular conformation. The parameters, *a, b, c, d,* and *e,* are weighting factors applied to raw energy terms. The interaction energy is then given by $\Delta G_{binding} = \Delta G_{FP} - (\Delta G_F + \Delta G_P)$.

In calculating Gibbs free energy, a room temperature of 298 K and an ionic strength of 0.5 of the "buffer" surrounding the protein were adopted. In order to correct the torsion angles and van der Waals clashes that may exist in the residues, a repair function from FoldX was used to further optimize the modeled structures. This facilitates the identification of other rotamers possible for the same residue. A new rotamer was kept only if FoldX predicted a more stable molecule, which avoided steric clashes in a specific position.

Label-Free Binding Assays. We further carried out binding assays based on a unique label-free biosensor to study the interactions between FvTox1 with different peptides. The biosensor utilizes a photonic crystal structure in a total-internal-reflection (PC-TIR) configuration, which has been demonstrated in our recent studies to offer ultrahigh detection sensitivity for quantifying molecular binding affinities.[11−15]

Fabrication of PC-TIR Sensors. Conventionally, a sharp resonant condition can be achieved with a high-Q optical microcavity with a cavity layer sandwiched by two pieces of PC structures. However, this conventional microcavity with a *closed* configuration is not suitable for biosensing, because it is difficult for analyte molecules to reach the sensing layer (cavity layer). For real-time binding assays, we open up the closed microcavity by using only one piece of the PC structure to form a cavity. Interestingly, we have obtained a sharp resonant condition by placing the single PC structure in a TIR configuration. Since there is a mirror image of the PC structure due to TIR, a microcavity is formed between the PC structure and its imaginary part. This unique configuration forms a PC-TIR sensor with an *open* sensing surface, which allows for easy immobilization of ligand molecules on the sensing surface and direct exposure of the functionalized sensor surface to analyte molecules for real-time bioassays.[11−15] In this study, PC-TIR sensors were designed and fabricated with electron beam physical vapor deposition. Each sensor consists of five alternating 89 nm TiO_2 and 305 nm SiO_2 layers coated on a BK-7 glass substrate. Above this periodic structure, a cavity layer was formed with 382 nm of SiO_2 and 10 nm of Si. When binding occurs on the PC-TIR sensor surface, the resonant angle of a probe laser beam will change accordingly, allowing for sensitive label-free binding assays.

Fabrication of a Microfluidic System. The open-cavity PC-TIR sensor offers a flat and smooth sensing surface, which allows for synergistic integration with a microfluidic system for injecting analyte samples onto the sensor chip. Polydimethylsiloxane (PDMS) microchannels were designed and fabricated using photolithography and replica molding. First, photoresist SU8-2025 (MicroChem) was spin coated on a clean silicon wafer to form a film thickness of 80 μm. A photomask with a pattern of five channels, each being 400 μm wide and 6 mm long, was then transferred onto the photoresist coated silicon wafer with a photolithography method to form a mold for making PDMS microchannels. A mixture of PDMS base and curing agents (Sylgard184, Dow Corning) at a ratio of 10:1 was degassed in a vacuum chamber to get rid of bubbles from the mixture before being cast on the mold. Microchannels were formed after the PDMS was cured overnight at 60 °C and separated from the mold. The PDMS microfluidic channels and a PC-TIR sensor chip were further processed with O_2 plasma for 30 s, producing hydrophilic surfaces for a tight and irreversible seal of the microchannels on the surface of the sensor chip. A syringe pump with five syringes was connected to the microchannels with Teflon tubing to control the flow rate of protein samples in TBS (Tris-buffered saline) or TBS buffer solutions onto the sensor chip.

Binding Experimental Setup. To measure the binding interaction of protein FvTox1 and putative FvTox1-interacting peptides (FvTox1-Protein; Table 1), the FvTox1 was first immobilized onto the surface of a sensor chip through electrostatic interactions, and fusion FvTox1-Protein solutions were then flowed through the microfluidic channels. A Helium−Neon laser was used as a probe light to monitor the change in the resonance condition of the functionalized PC-TIR sensor due to biomolecular bindings. The probe laser beam was first expanded to 10 mm with a pair of lenses before it was focused with a cylindrical lens into a line crossing the five microchannels on the sensor surface. The reflected beam was collimated with another cylindrical lens and imaged onto a CCD camera (Figure 1).

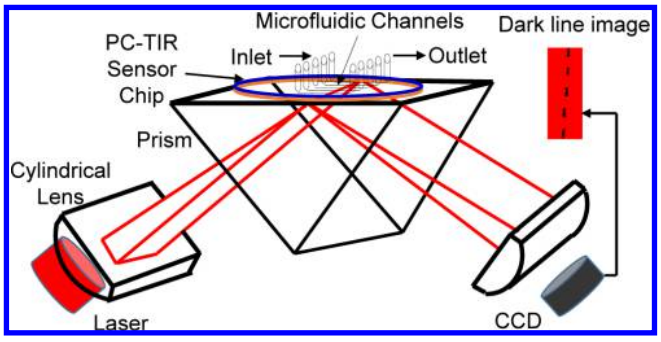

Figure 1. Schematic diagram of the experimental setup. A microfluidic system is coupled with a PC-TIR sensor. Resonant dark lines of a reflected probe laser beam from the sensor corresponding to the five microchannels can be monitored with a CCD camera.

Five dark lines were observed in the image, which correspond to the resonant angle of the probe beam for each of the five microchannels of the PC-TIR sensor. When the analyte fusion FvTox1-Protein solutions flow through the channels and peptides interacted with the FvTox1 molecules immobilized on the sensor surface, the positions of the dark lines shifted accordingly based on the binding strengths.

To correlate the shifts of the dark lines in pixel numbers with the changes of the resonant wavelength of the sensor, we compared the results of standard solutions measured by the angular modulation mode with that from a spectral modulation mode. For the measurements of the resonant wavelength, a broadband white light source was coupled to a single-mode optical fiber, and the output light from the fiber was collimated with an aspherical lens and passed through a linear polarizer to select s-polarization.[24] The light had an incident angle of 64° to a PC-TIR sensor, and the spectra of the beam reflected from the sensor were measured with a high-resolution spectrometer (HR4000, Ocean Optics) to monitor the resonant wavelength.

DOI: 10.1021/acs.analchem.5b02442
Anal. Chem. XXXX, XXX, XXX−XXX

Mixtures of ethylene glycol and water at different ratios were used as standard solutions and injected into microchannels on the sensor. The changes in the resonant wavelength were recorded and compared to the shift in the dark line positions obtained from the imaging setup to convert the dark line position changes to resonant wavelength shifts.

The angular-modulation of the label-free bioassay setup (Figure 1) was used to measure the interactions of FvTox1 with different fusion FvTox1-Protein samples according to the protocol described below. First, Tris-buffered saline (TBS, pH 7.4) solution flowed at a speed of 5 μL/min in all microchannels on the sensor chip. The dark line position for each channel was recorded to establish the corresponding detection baseline. Second, the TBS buffer solutions in four channels were replaced with FvTox1 solutions in TBS (0.8 μM, 200 μL), while the fifth channel served as the reference with continuous flow of a TBS solution. The shifts of dark lines for different channels were recorded in real-time, which reflect the amount of FvTox1 molecules immobilized on the sensor surface. Third, the sensor surface was washed by flowing TBS through the channels. The positions of the dark lines were recorded again. By comparing the net shifts of the dark lines with the detection baseline, the amount of FvTox1 molecules immobilized onto the sensor surface was quantified. Finally, the four channels were flowing with the fusion FvTox1-Protein solutions in TBS (2.9 μM, 200 μL), while keeping the reference channel flowing with a TBS buffer solution. The amount of peptide molecules captured by the FvTox1 bound to the sensor surface can be obtained by calculating the shifts of the dark lines.

RESULTS AND DISCUSSION

Bioinformatics Calculation Results. The molecular structures of FvTox1 and the four fusion FvTox1-Proteins, each containing a unique putative FvTox1-interacting peptide isolated by screening a phage display library calculated with the $(PS)^2$ server based on their amino acid sequences (Table 1), are shown in Figure 2.

To further predict the complex structures due to the interaction between FvTox1 and the four FvTox1-Proteins, we utilized the ClusPro server, which allows one to predict the putative structures of FvTox1−FvTox1-Protein complexes by calculating the docking strengths. Because there is no prior knowledge of what forces dominate in the FvTox1−FvTox1-Protein complexes, we utilized the calculation option supported by ClusPro, which assumes balanced coefficients for taking into account different intermolecular forces. The ClusPro docking algorithm starts with evaluating billions of putative complexes and narrows them down to a number of structures (typically 2000 to 20 000) with favorable surface complementarities. A free energy filtering algorithm is then applied to this set of structures to select those exhibiting favorable electrostatic and desolvation free energies. The selected energetically favorable structures are further clustered to generate a short list of putative complexes, ranked based on cluster sizes. The ClusPro algorithm is one of the most powerful approaches for predicting protein−protein docking.[17−20] Nevertheless, the accuracy of theoretical predictions of complicated protein complexes based on bioinformatics calculations is generally limited. This is because bioinformatic methods typically have to utilize different assumptions in calculations that may oversimplify molecular structures and interactions. For example, it may include the assumption that similar types of chemical bonds have equal strength and there are no intra-aggregate reactions yielding cyclical structures.[25−27]

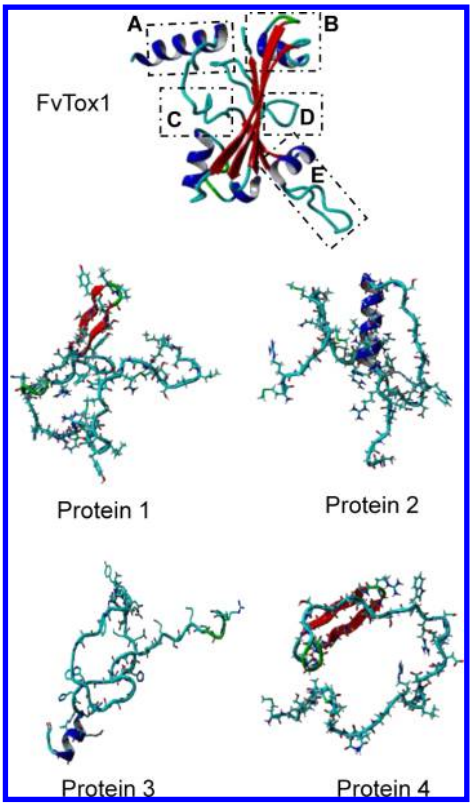

Figure 2. Calculated molecular structures of FvTox1 and four interacting FvTox1-Proteins (Table 1). Different regions A−E of FvTox1 are marked with dashed lines for easy discussion in the next section about the bindings between FvTox1 and the proteins containing FvTox1 interacting peptides.

At present, there is not a single bioinformatics model by which one could predict precisely the structure of a protein complex from a mixture of its component proteins. Therefore, for each FvTox1−FvTox1-Protein binding pair, we selected the top 20 ranked putative complex structures predicted with the ClusPro algorithm to further calculate their binding energies, thus optimizing the prediction of the FvTox1−FvTox1-Protein complexes.

We utilized the FoldX modeling algorithm[21−23] to compute the Gibbs free energies of different putative FvTox1−FvTox1-Protein complexes (Figure 3). It can be seen that, among the top 20 ranked putative complexes of FvTox1 and FvTox1-Protein 3, nearly 50% of the complexes are of positive Gibbs free energies; therefore, half of these complexes are not stable, while 70% and 75% of FvTox1 and FvTox1-Protein 1 complex and FvTox1 and FvTox1-Protein 4 complex, respectively, are of negative Gibbs free energies, indicating the possible stable complex structures. Especially, for the FvTox1-Protein 2 interactions, the number of the stable complexes reaches 85%, which suggests the highest possibility for a strong binding between FvTox1 and FvTox1-Protein 2.

The ranking of the putative complexes predicted with the ClusPro docking algorithm is based on minimization of cluster sizes. To balance the interplay between structure and energy, for FvTox1 interacting with each FvTox1-Protein, the most favorable complex was selected from the top five ranked putative complexes predicted by the ClusPro algorithm and having the lowest interaction energy. The final results of the predicted structures and interaction energies of FvTox1−FvTox1-Protein complexes are summarized in Figure 4. The interacting

DOI: 10.1021/acs.analchem.5b02442
Anal. Chem. XXXX, XXX, XXX−XXX

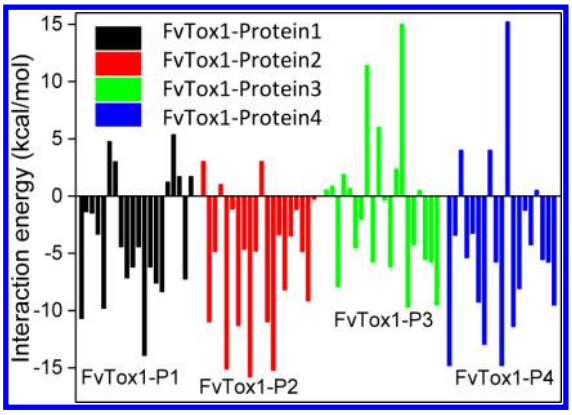

Figure 3. Calculated interaction energies of FvTox1 interacting with four different putative FvTox1-Proteins (Table 1). For each interacting pair, the top 20 ranked complexes obtained from ClusPro predictions were selected for calculation of the interaction energies of the putative structures. P1, Protein 1; P2, Protein 2; P3, Protein 3; P4, Protein 4.

regions of FvTox1 with FvTox1-Protein 1 are located at regions A and C of FvTox1 (the regions of FvTox1 are marked in Figure 2). The interacting region of FvTox1 and FvTox1-Protein 2 fully covers areas B, D, and E, thereby illustrating that almost a half side area of FvTox1 is interacting with FvTox1-Protein 2. The interacting area of FvTox1 with FvTox1-Protein 3 just covers area B and a small section of area D. As for FvTox1 and FvTox1-Protein 4, the interacting region covers areas A, B, C, and D. Obviously, the interacting area of FvTox1 and FvTox1-Protein 3 is the smallest among these four FvTox1−FvTox1-Protein complexes, suggesting the weakest binding interaction. The calculated interaction energy corresponding to the most stable structure for each complex is also shown in Figure 4. The interaction energy of FvTox1 and FvTox1-Protein 2 is the lowest one with a value of only −15.80 kcal/mol, while those of FvTox1 with FvTox1-Protein 1, 3, and 4 are −13.92, −7.93, and −14.81 kcal/mol, respectively. These results indicate that the binding strength between FvTox1 and FvTox1-Protein 2 is the strongest, while that of FvTox1 and FvTox1-Protein 3 is the weakest.

Experimental Results of FvTox1−FvTox1-Protein Interactions. To validate the bioinformatics prediction of FvTox1−FvTox1-Protein interacting energies, we have conducted binding assays of FvTox1 with the four FvTox1-Proteins using our PC-TIR label-free biosensor system. In order to obtain the baseline data, TBS buffer solutions were first injected into all the five microchannels on the surface of a PC-TIR sensor chip. An image of the resonant dark lines of a probe laser beam reflected off the PC-TIR sensor is shown in Figure 5a,

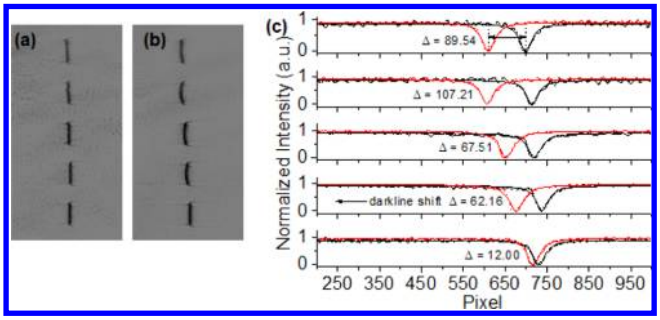

Figure 5. (a) An image of resonant dark lines of a probe laser beam reflected from the PC-TIR sensor with five microchannels flowing with TBS buffer solutions. (b) An example image showing that the dark lines corresponding to four channels shifted after they were treated with FvTox1 solutions and bound with four different peptides. (c) Example intensity profiles of the dark lines corresponding to the five channels before (black) and after (red) the bindings. Lorentzian functions were used to fit the curves and obtain the precise values of the shifts.

which indicates the detection baseline for the five microchannels. FvTox1 solutions in TBS were then used to replace the buffer solutions in four microchannels to immobilize FvTox1 onto the sensor surface, thereby forming a targeting

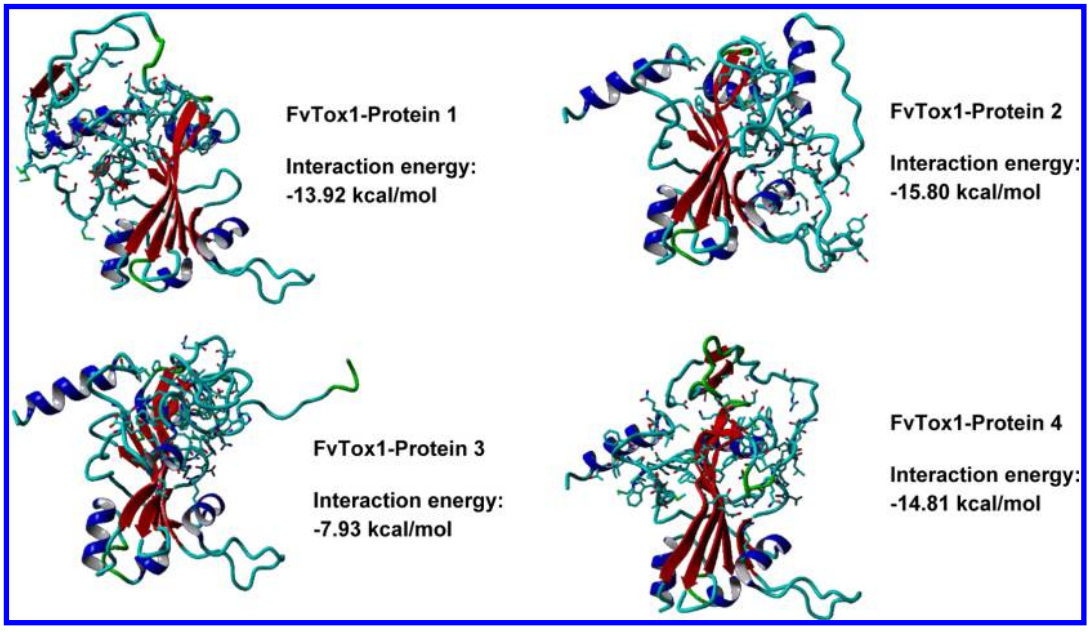

Figure 4. Structures and interaction energies of the complexes between FvTox1 and the four FvTox1-interacting peptides as fusion FvTox1-Proteins (Table 1). The results indicate that FvTox1 and FvTox1-Protein 2 containing FvTox1-interacting Peptide 2 form the most stable structure compared with the other three complexes.

DOI: 10.1021/acs.analchem.5b02442
Anal. Chem. XXXX, XXX, XXX−XXX

layer for FvTox1-Proteins, while leaving one channel as the reference with continuous flow of TBS. After washing away the excess FvTox1 from the channels with TBS, we injected the four different FvTox1-Proteins (Table 1) containing FvTox1-interacting peptides as fusion FvTox1-Proteins into the channels. The resonant dark lines start shifting with time. Figure 5b shows a representative image of the dark lines. In order to find out the precise amount of shifts relative to the baseline, we plotted the intensity profile of each dark line and fit the curve with a Lorentzian function (Figure 5c). The resonant dark line of the reference channel had a shift of 12 pixels, which may be attributed to a combined effect due to temperature fluctuations and mechanical drifting problems. The net changes of the signal channels were obtained by subtracting the reference shift.

Figure 6 summaries the binding assay results of FvTox1 with four fusion FvTox1-Proteins containing four FvTox1-interacting

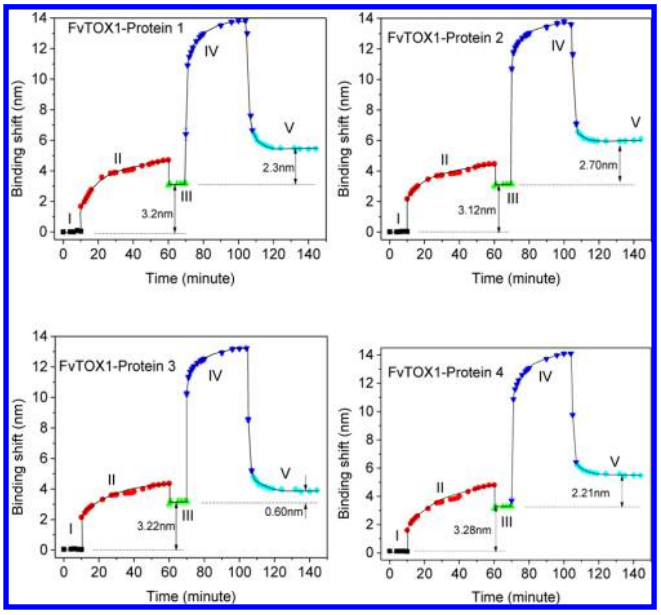

Figure 6. Label-free binding assay results of FvTox1 interacting with the four fusion proteins carrying peptides of interest. Stage I: TBS buffer solution baseline; Stage II: Immobilization process of FvTox1 onto the sensor surface; Stage III: Net binding shifts due to immobilized FvTox1 after TBS wash; Stage IV: FvTox1-peptide binding kinetics; Stage V: Net binding shifts of the peptides with FvTox1 after TBS wash. The concentration of FvTox1 used was 0.8 μM, and its total volume was 200 μL. The recombinant FvTox1-proteins 1 through 4 (Table 1) used had a concentration of 2.9 μM and a volume of 200 μL. The flow speed for all the samples was 5 μL/min.

peptides. The shifts in pixel numbers were converted to the changes in resonant wavelength in nanometers based on the measurements of standard solutions using both the angular modulation and spectrum detection.[11] The curves of Stage I in Figure 6 show the detection baseline of the PC-TIR sensor when TBS was flowing in the microfluidic channels on the sensor chip surface. Stage II shows the results of the process of immobilizing FvTox1 on the chip surface, while Stage III shows that the net binding shift of FvTox1 is about 3.2 nm after the TBS wash. Stage IV shows large shifts when the fusion FvTox1-Proteins containing FvTox1-interacting peptides were injected onto the sensor surface through the microchannels. The shifts are in part due to the binding of the FvTox1-Proteins onto the functionalized sensor surface and in part due to the bulk solution effect as the peptide solutions have higher refractive indices than that of TBS. TBS buffer solutions were then injected into the microchannels to replace the FvTox1-interacting peptide solutions to wash away the loosely bound peptide molecules. Since the refractive index of the bulk solution returned to that of TBS, the net shifts shown in Stage V were due to the binding of the FvTox1-Protein with FvTox1. The interaction of FvTox1 and FvTox1-Protein 3 is obviously much weaker than those of the other three FvTox1-Proteins with FvTox1. The interaction strength of FvTox1 and FvTox1-Protein 2 containing FvTox1-interacting Peptide 2 is the strongest among the four fusion FvTox1-Proteins carrying FvTox1-interacting peptides.

The objective of this study is to identify an FvTox1-Protein that shows the strongest interaction with FvTox1 in order to open up the possibility for partially neutralizing the toxic effect of FvTox1 *in planta* for generating SDS resistant transgenic soybean plants. As indicated by our molecular simulations, the interaction energy of FvTox1 with FvTox1-Protein 2 containing FvTox1-interacting peptide 2 has a value of −15.80 kcal/mol, the lowest one among the four peptides under study. Thus, both the label-free binding assays and the molecular simulations revealed that the binding strength of FvTox1 with FvTox1-Protein 2 is the strongest. However, as in the molecular simulation study, the interactions of FvTox1 with FvTox1-Proteins 1 and 4 were very comparable, whereas interaction of the FvTox1 toxin with FvTox1-Protein 3 is the weakest. The molecular simulations and the label-free binding assays cross-validated each other with a significantly strong association (r = 0.99) between the outcomes of the two approaches (Figure 7).

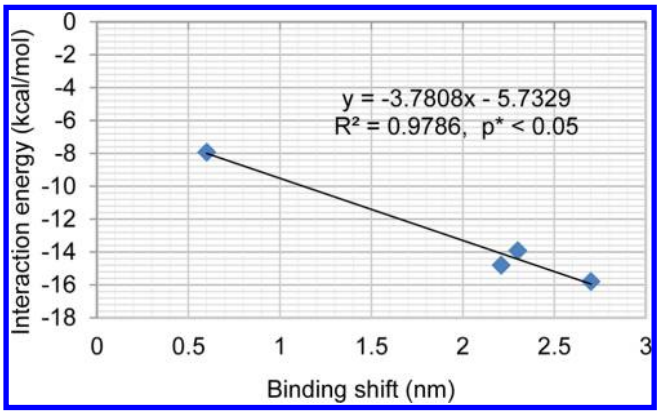

Figure 7. Relationship between interaction energy calculated by bioinformatics approaches and binding shift measured by a PC-TIR biosensor as interaction strengths of FvTox1 interacting peptides with FvTox1. The data for this association study are taken from Figures 4 and 6. The association (r) between the two sets of data is 0.99. The asterisk means statistical significance.

It is however essential to cross validate the *in vitro* interaction of FvTox1 with the identified peptides in an additional quantitative *in vitro* binding assay, where dissociation constants (K_d) between FvTox1 with four FvTox1-Proteins can be determined using a range of μM solutions.[28] Unfortunately, due to the lack of sufficient amounts of the purified fusion FvTox1-Proteins containing the FvTox1-interacting peptides, we were not able to conduct such an assay.

The *in vitro* interaction data presented here indicate the candidate FvTox1-interacting peptides that are suitable for further evaluation to determine their possible role in neutralizing

DOI: 10.1021/acs.analchem.5b02442
Anal. Chem. XXXX, XXX, XXX−XXX

the FvTox1 toxin in transgenic soybean plants. We anticipate that, since FvTox1 is the major toxin for foliar SDS development, strong FvTox1-interacting peptides expressed in transgenic soybean plants will be able to neutralize FvTox1 resulting in SDS resistant soybean cultivars.[3]

CONCLUSIONS

The interactions of FvTox1 with four fusion proteins FvTox1-Proteins 1, 2, 3, and 4 containing four distinct synthetic peptides (Table 1) screened from phage peptide libraries were predicted by bioinformatics molecular simulations and then investigated with a label-free photonic crystal biosensor. Both the theoretical and experimental results indicate that, among the four FvTox1-proteins, the interaction of FvTox1 with FvTox1-Protein 3 is the weakest, while the interaction strength of FvTox1 with FvTox1-Protein 2 is the strongest. Although bioinformatics calculations alone may not be overwhelmingly convincing in the prediction of protein−peptide interactions, the presented information regarding the interaction of FvTox1 with FvTox1-Proteins *in vitro* obtained from our label free protein−protein interaction assays corroborated with the bioinformatics-based calculations. These results indicated that most likely FvTox1-Proteins 1, 2, and 4 are suitable to explore for their possible *in planta* interactions with FvTox1 following *F. virguliforme* infection in transgenic soybean lines. A strong *in planta* interaction between FvTox1 with any of these three FvTox1-Proteins may result in foliar SDS resistance in transgenic soybean cultivars. This study also implies that bioinformatics-based prediction of protein−peptide interaction could be considered for evaluation of a large number of protein−protein interactions.

AUTHOR INFORMATION

Corresponding Author

*E-mail: jingyong.ye@utsa.edu.

Notes

The authors declare no competing financial interest.

ACKNOWLEDGMENTS

We acknowledge the grant support from USDA NIFA 2013-68004-20374 and San Antonio Life Sciences Institute Academy.

REFERENCES

(1) Aoki, T.; O'Donnell, K.; Homma, Y.; Lattanzi, A. R. *Mycologia* **2003**, *95*, 660−684.
(2) Pudake, R. N.; Swaminathan, S.; Sahu, B. B.; Leandro, L. F.; Bhattacharyya, M. K. *Curr. Genet.* **2013**, *59*, 107−117.
(3) Brar, H. K.; Bhattacharyya, M. K. *Mol. Plant-Microbe Interact.* **2012**, *25*, 817−824.
(4) Wang, B.; Swaminathan, S.; Bhattacharyya, M. K. *PLoS One* **2015**, *10*, e0145156.
(5) Chen, C. C.; Hwang, J. K.; Yang, J. M. *Nucleic Acids Res.* **2006**, *34*, W152−W157.
(6) Chen, C. C.; Hwang, J. K.; Yang, J. M. *BMC Bioinf.* **2009**, *10*, 366.
(7) Zemla, A. *Nucleic Acids Res.* **2003**, *31*, 3370−3374.
(8) Berggard, T.; Linse, S.; James, P. *Proteomics* **2007**, *7*, 2833−2842.
(9) Schneider, B. H.; Edwards, J. G.; Hartman, N. F. *Clinical Chemistry* **1997**, *43*, 1757−1763.
(10) Fan, X. D.; White, I. M.; Shopova, S. I.; Zhu, H. Y.; Suter, J. D.; Sun, Y. Z. *Anal. Chim. Acta* **2008**, *620*, 8−26.
(11) Zhang, B.; Morales, A. W.; Peterson, R.; Tang, L.; Ye, J. Y. *Biosens. Bioelectron.* **2014**, *58*, 107−113.
(12) Zhang, B.; Tamez-Vela, J.; Solis, S.; Bustamante, B.; Peterson, R.; Rahman, S.; Morales, A.; Tang, L.; Ye, J. Y. *Journal of Medical Engineering* **2013**, *2013*, 808056.
(13) Zhang, B.; Dallo, S.; Peterson, R.; Hussain, S.; Weitao, T.; Ye, J. Y. *J. Biomed. Opt.* **2011**, *16*, 127006.
(14) Guo, Y.; Ye, J. Y.; Divin, C.; Thomas, T. P.; Myc, A.; Bersano-Begey, T. F.; Baker, J. R., Jr.; Norris, T. B. *Anal. Chem.* **2010**, *82*, 5211−5218.
(15) Guo, Y. B.; Divin, C.; Myc, A.; Terry, F. L.; Baker, J. R.; Norris, T. B.; Ye, J. Y. *Opt. Express* **2008**, *16*, 11741−11749.
(16) Tress, M.; Ezkurdia, L.; Grana, O.; Lopez, G.; Valencia, A. *Proteins: Struct., Funct., Genet.* **2005**, *61*, 27−45.
(17) Kozakov, D.; Beglov, D.; Bohnuud, T.; Mottarella, S. E.; Xia, B.; Hall, D. R.; Vajda, S. *Proteins: Struct., Funct., Genet.* **2013**, *81*, 2159−2166.
(18) Kozakov, D.; Brenke, R.; Comeau, S. R.; Vajda, S. *Proteins: Struct., Funct., Genet.* **2006**, *65*, 392−406.
(19) Comeau, S. R.; Gatchell, D. W.; Vajda, S.; Camacho, C. J. *Bioinformatics* **2004**, *20*, 45−50.
(20) Comeau, S. R.; Gatchell, D. W.; Vajda, S.; Camacho, C. J. *Nucleic Acids Res.* **2004**, *32*, W96−99.
(21) Schymkowitz, J.; Borg, J.; Stricher, F.; Nys, R.; Rousseau, F.; Serrano, L. *Nucleic Acids Res.* **2005**, *33*, W382−W388.
(22) Guerois, R.; Nielsen, J. E.; Serrano, L. *J. Mol. Biol.* **2002**, *320*, 369−387.
(23) Kiel, C.; Serrano, L.; Herrmann, C. *J. Mol. Biol.* **2004**, *340*, 1039−1058.
(24) Zhang, B. L.; Dallo, S.; Peterson, R.; Hussain, S.; Tao, W. T.; Ye, J. Y. *J. Biomed. Opt.* **2011**, *16*, 127006.
(25) Bray, D.; Lay, S. *Proc. Natl. Acad. Sci. U. S. A.* **1997**, *94*, 13493−13498.
(26) Goldberg, R. J. *J. Am. Chem. Soc.* **1953**, *75*, 3127−3131.
(27) Goldberg, R. J. *J. Am. Chem. Soc.* **1952**, *74*, 5715−5725.
(28) Orosz, F.; Ovadi, J. *J. Immunol. Methods* **2002**, *270*, 155−162.

DOI: 10.1021/acs.analchem.5b02442
Anal. Chem. XXXX, XXX, XXX−XXX